In-situ observation of magnetization reversal process of Sm(Co,Cu,Fe,Zr)$_z$ magnets with different Fe contents

Shuo Wu [ORCID] **, Dong-Tao Zhang, Ming Yue*** [ORCID] **, Yun-Qiao Wang, Zhi-Feng Shang, Dan Wu, Jing-Ming Liang**

Abstract Sm(Co,Cu,Fe,Zr)$_z$ magnets have drawn much attention for high-temperature applications due to their high Curie temperature, strong corrosion resistance and thermal stability. The effect of increasing Fe content on the distribution of elements and squareness (S_r) of demagnetization curves were investigated for two kinds of magnets with different nominal compositions of Sm(Co$_{bal}$Fe$_{0.15}$Cu$_{0.07}$Zr$_{0.03}$)$_{7.8}$ and Sm(Co$_{bal}$Fe$_{0.28}$Cu$_{0.07}$Zr$_{0.03}$)$_{6.6}$ in this work. The magnetic properties of the magnets with higher Fe content fluctuate greatly after different solution treatments, indicating that they are more sensitive to the process temperature. The increase in Fe content can obviously enhance the cellular phase size. Meanwhile, inhomogeneous Cu distribution is observed in the Sm(Co$_{bal}$Fe$_{0.28}$Cu$_{0.07}$Zr$_{0.03}$)$_{6.6}$ magnet, resulting in the different cellular structures and corresponding magnetic domain patterns in different regions in the inner grains. Furthermore, the lower Cu content regions are responsible for the wider magnetic domain, which have weaker resistance to applied magnetic field. As a result, S_r of demagnetization curve decreases with the increase in Fe content due to the inhomogeneous Cu distribution, which was confirmed by in-situ observation of electron probe micro-analyzer (EPMA) and magneto-optical Kerr optical microscope (MOKE).

Keywords Sm(Co,Cu,Fe,Zr)$_z$ magnets; Cu distribution; Microstructure; Magnetic properties; Magnetic domain; Squareness

S. Wu, D.-T. Zhang, M. Yue*, Y.-Q. Wang, Z.-F. Shang, D. Wu, J.-M. Liang
College of Materials Science and Engineering, Key Laboratory of Advanced Functional Materials, Ministry of Education of China, Beijing University of Technology, Beijing 100124, China
e-mail: yueming@bjut.edu.cn

1 Introduction

Sm(Co,Fe,Cu,Zr)$_z$ magnets are widely used in aerospace, defense, military and other fields due to their high Curie temperature, excellent thermal stability and corrosion resistance [1–7]. The 2:17-type SmCo sintered magnets have complex microstructure, consisting of Sm$_2$(Co,Fe)$_{17}$ rhombohedral phase, Sm(Co,Cu)$_5$ hexagonal phase and Zr-rich lamellar phase with hexagonal phase [8–11]. The Sm$_2$(Co,Fe)$_{17}$ phase is responsible for high remanence (B_r) [12–18]. The increase in the concentration gradient of Cu content between the Sm$_2$Co$_{17}$ phase and the SmCo$_5$ phase enhances the domain wall pinning. In addition, Zr-rich lamellar phase provides a path for Cu atoms to diffuse into the cell boundary phase, leading to the increase in the coercivity (H_{cj}) [19–22].

The increase in Fe content of the magnet can effectively enhance its saturation magnetization and promote the growth of 2:17R cellular phase, resulting in the decrease in content of 1:5H cell boundary phase [23]. However, if Fe content is too high, the integrity of cell boundary phase would be destroyed [24–26]. Thus, the content of Sm should be increased to maintain the volume of 1:5H phase [27]. In addition, the magnetic properties of the 2:17-type SmCo magnets are extremely sensitive to the variation of the composition. Inhomogeneity of element distribution can lead to the damage of squareness (S_r) and the reversal process of magnetic domain [28]. Therefore, it is necessary to investigate the elemental distribution and the magnetic domain in the magnets, which will possibly reveal the relationship between microstructure and S_r of demagnetization curve.

In this paper, Sm(Co$_{bal}$Fe$_{0.15}$Cu$_{0.07}$Zr$_{0.03}$)$_{7.8}$ magnets and Sm(Co$_{bal}$Fe$_{0.28}$Cu$_{0.07}$Zr$_{0.03}$)$_{6.6}$ magnets were prepared. The effect of Cu distribution on micromorphology and

magnetic domain was studied by in-situ observation through electron probe micro-analyzer (EPMA) and magneto-optical Kerr optical microscope (MOKE). This in-situ observation can provide more intuitive images, which can effectively reveal the relationship between microstructure and magnetic properties.

2 Experimental

Two kinds of magnetic alloy ingots with nominal compositions of Sm(Co$_{bal}$Fe$_{0.15}$Cu$_{0.07}$Zr$_{0.03}$)$_{7.8}$ (named M$_A$ magnet) and Sm(Co$_{bal}$Fe$_{0.28}$Cu$_{0.07}$Zr$_{0.03}$)$_{6.6}$ (named M$_B$ magnet) were prepared by the induction melting method, and their nominal compositions are listed in Table 1. The ingots were crashed and ball-milled into single crystal powders. The obtained powders were pressed under a magnetic field of 1600 kA·m^{-1}, and then isostatically compacted under a pressure of 230 MPa for 120 s. The green bodies of M$_A$ magnet and M$_B$ magnet were sintered at 1488 K for 1 h, then the solid solution was performed at 1423–1443 K for 2.5 h. Final isothermal aging was performed at 1083 K for 40 h followed by slow cooling down to 693 K at a rate of 0.4 K·min^{-1}, and then, the magnets were aged at 693 K for 10 h before cooling to room temperature.

Magnetic properties of the magnets were tested using NIM-500C B-H hysteresis loop tracer with magnetic field up to 2400 kA·m^{-1}. The magnets were observed using FEI NOVA nano2000 scanning electron microscope (SEM), and equipped with energy-dispersive spectroscopy (EDS). The Cu distribution in the magnets was analyzed by EPMA-1720 with a wavelength-dispersive X-ray (WDX) detector. The magnetic domain structure and microstructure were observed by BH-786IP-PK-type MOKE and transmission electron microscope (TEM), respectively. A JEM-2010-type TEM was used in this work.

3 Results and discussion

Figure 1 shows the magnetic properties of the M$_A$ and M$_B$ magnets at different solid solution temperatures. It is found that the magnetic properties change drastically with the

Table 1 Nominal compositions of Sm(Co$_{bal}$Fe$_{0.15}$Cu$_{0.07}$Zr$_{0.03}$)$_{7.8}$ and Sm(Co$_{bal}$Fe$_{0.28}$Cu$_{0.07}$Zr$_{0.03}$)$_{6.6}$ (wt%)

Magnets	Sm	Co	Fe	Cu	Zr
M$_A$	24.39	55.92	10.60	5.63	3.46
M$_B$	27.14	44.85	19.19	5.46	3.36

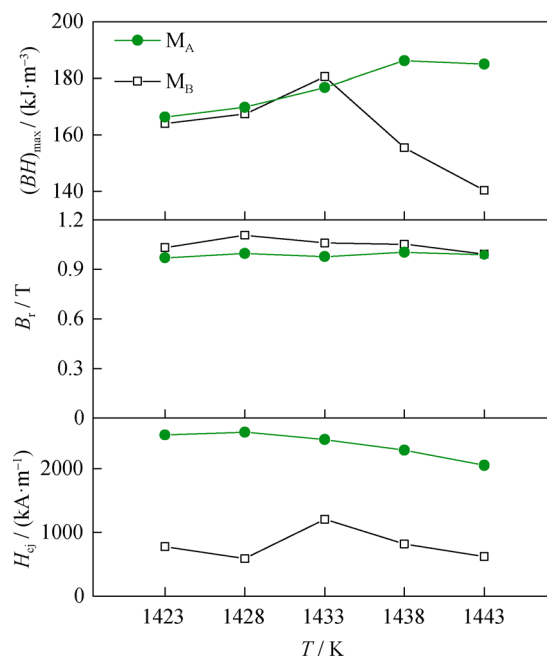**Fig. 1** Main magnetic properties of sintered Sm(CoFeCuZr)$_z$ magnets at different solid solution temperatures

solid solution temperature increasing, indicating that the solid solution temperature plays a key role in determining the magnetic properties. H_{cj} and B_r of both M$_A$ and M$_B$ magnets significantly fluctuate with the temperature, and the remanence of M$_B$ magnet is higher than that of M$_A$ magnet. The maximum energy product ((BH)$_{max}$) of 185.27 kJ·m^{-3} for M$_A$ magnet and 179.74 kJ·m^{-3} for M$_B$ magnet are achieved at different temperatures of 1438 K and 1433 K, respectively. The optimal (BH)$_{max}$ of M_B magnet is lower than that of M$_A$ magnet, which can be contributed to its lower S_r of 80.20%.

Figure 2 shows the demagnetization curves of M$_A$ and M$_B$ magnets at their optimal temperature, and corresponding magnetic properties are listed in Table 2. In Fig. 2, a small step appears in the demagnetization curve of M$_A$ magnet at the applied field of about − 560 kA·m^{-1}, but the curve tends to be smooth when the field exceeds − 800 kA·m^{-1}. For M$_B$ magnet, the demagnetization curve is smooth before − 400 kA·m^{-1}, then drops sharply
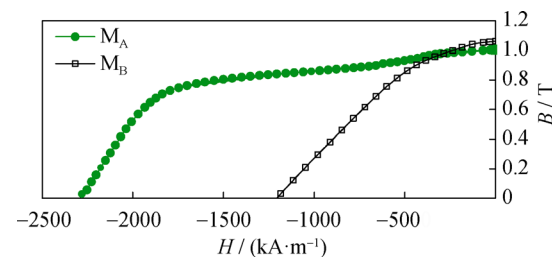

Fig. 2 Demagnetization curves of M$_A$ magnet and M$_B$ magnet

Table 2 Magnetic properties of M_A and M_B magnets

Magnets	B_r/T	H_{cj}/(kA·m^{-1})	$(BH)_{max}$/(kJ·m^{-3})	S_r/%
M_A	1.005	2287.2	185.27	92.20
M_B	1.061	1200.0	179.73	80.20

and becomes zero at about − 1200 kA·m^{-1}. Although the B_r of M_B magnet is slightly higher than that of M_A magnet, the S_r of demagnetization curve of M_A magnet is obviously better than that of M_B magnet, leading to a larger $(BH)_{max}$ of M_A magnet. As can be seen from Table 1, the contents of the remaining elements are very similar except for the different contents of Sm and Fe in these two alloys. The intrinsic magnetic properties and the microstructure of the magnets are two main factors affecting the magnetic properties. It is generally believed that increasing Fe content is an important way to increase the $(BH)_{max}$ at room temperature. The magnetic properties of M_B magnet fluctuate greatly with the change in solution temperature, indicating that the magnet with higher Fe content is more sensitive to the heat treatment.

To investigate the relationship between the poor S_r and inhomogeneous microstructure, M_A magnet was observed by in-situ SEM, EPMA and MOKE. Figure 3a shows the back-scattered electron (BSE) image of the M_A magnet, in which the grain boundaries and the Sm_2O_3 phase can be observed. Figure 3b shows the distribution of Cu observed by EPMA. It is found that the distribution of Cu in grains is homogeneous. Besides, the Cu-lean phenomenon at the grain boundaries is also observed, which agrees with the previously reported results by Wang et al. [29]. The image

of the thermal demagnetization state (TDS) of M_A magnet is shown in Fig. 3c. The width of the maze-like magnetic domain is about 1.5 μm. And the magnetic domain width decreases with the increase in Cu content. Magnetic domain width in different regions of M_A magnet is similar due to the uniform distribution of Cu [30]. Figure 3d–h shows the magnetic domain images of M_A magnet at reversal magnetic field of 0, − 400, − 560, − 800 and − 1120 kA·m^{-1}, respectively. In Fig. 2, the demagnetization curve of M_A magnet presents a small step from 0 to − 560 kA·m^{-1}. When the demagnetizing field of − 400 kA·m^{-1} was applied, the magnetic domain at grain boundary is not deflected completely yet and no obvious change in the magnetic domain of the inner grains is observed. When the reversal magnetic field applied increases to − 560 kA·m^{-1}, the magnetic domain at grain boundary with lower Cu content deflects basically, and there is still no obvious magnetic domain deflection in the grain, which is the direct reason for the observed step in the demagnetization curve of M_A magnet. When the reverse field increases to − 800 kA·m^{-1}, there are scattered reverse magnetic domains inside the grains. With the enlargement of the reverse magnetic field to − 1120 kA·m^{-1}, the distribution of the reverse domains becomes uniform in the grains. It is noticed that the H_{cj} of the sample is 2400 kA·m^{-1}, but the maximum magnetic field for the MOKE observation is only 1160 kA·m^{-1}. Therefore, this indicates that the uniformity of composition between grains has an influence on the magnetic domain structure and the S_r of demagnetization curve.

Figure 4a shows BSE image of M_B magnet where the observation surfaces were perpendicular to c-axis of the magnets. Three distinct phases named as gray 2:17 main
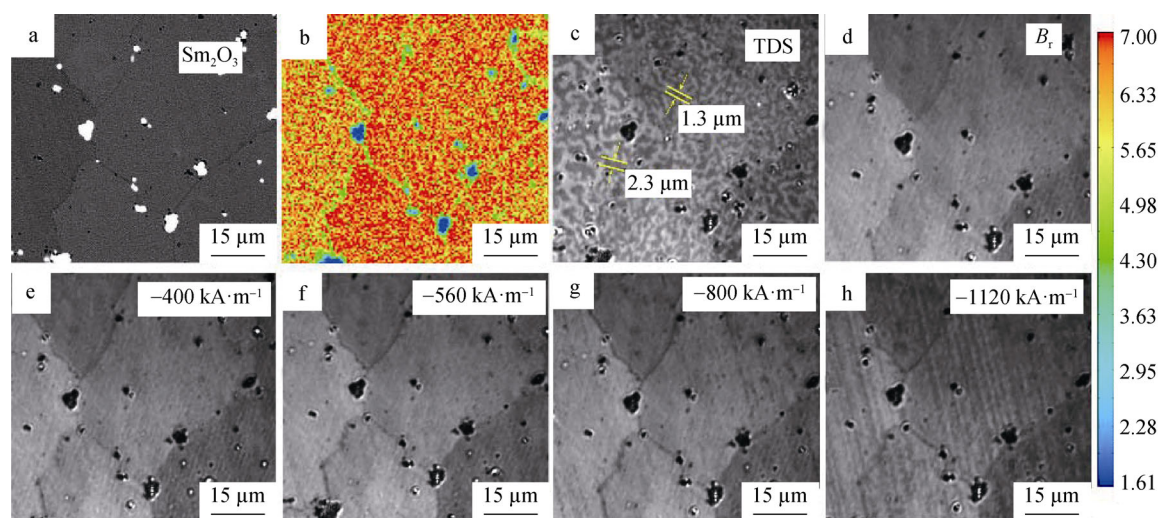

Fig. 3 In-situ observations of M_A magnet: **a** BSE image; **b** Cu-mapping image (Cu content shown with right scale bar); magnetic domain images at **c** thermal demagnetization state (TDS) and **d** remanence state (B_r); magnetic domain images at reversal magnetic fields of **e** − 400 kA·m^{-1}, **f** − 560 kA·m^{-1}, **g** − 800 kA·m^{-1} and **h** − 1120 kA·m^{-1}
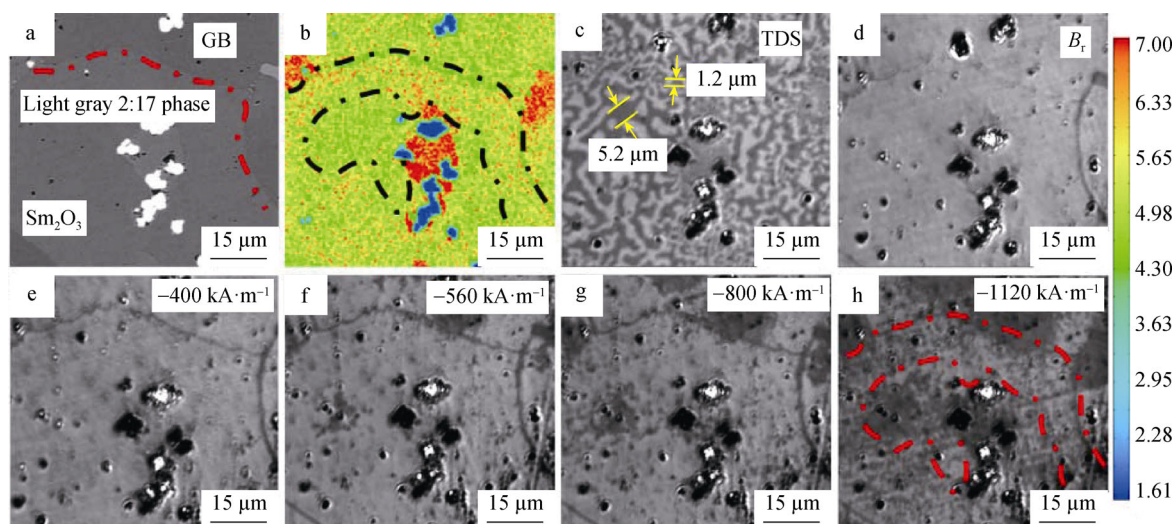
Fig. 4 In-situ observations of M$_B$ magnet: **a** BSE image; **b** Cu-mapping image (Cu content shown with right scale bar); magnetic domain images at **c** thermal demagnetization state (TDS) and **d** remanence state (B_r); magnetic domain images at reversal magnetic fields of **e** $-$ 400 kA·m^{-1}, **f** $-$ 560 kA·m^{-1}, **g** $-$ 800 kA·m^{-1} and **h** $-$ 1120 kA·m^{-1}

phase, white Sm$_2$O$_3$ phase and light gray 2:17 phase can be seen. Figure 4b shows corresponding EPMA result of Fig. 4a, and the phenomenon of Cu-lean at grain boundaries is clearly observed. The elemental distribution is obviously different from that of the M$_A$ magnet. In the grain marked by dotted line, the content of Cu in the light gray 2:17 phase is much higher than that near the grain boundary, while the Cu content in the middle region of grain is less. Figure 4c shows magnetic domain of M$_B$ magnet at TDS. Many studies have reported that concentration gradient of Cu between cell boundary phase and cellular phase can obviously influence the magnetic domain patterns in the 2:17-type SmCo sintered magnets [31]. Cu content is inversely proportional to magnetic domain thickness, which suggests that domain width is determined by microstructure and microchemistry. The domain width in grains ranges from 1 to 5 μm, as shown in Fig. 4b. Therefore, the magnetic domains with different widths may not reverse at the same reversal magnetic field, as shown in Fig. 4c. Figure 4d shows the magnetic domain pattern at the remanence state. Only, part of the magnetic domain at the grain boundaries is reversed firstly, resulting from its low Cu content. When the demagnetized field applied increases to $-$ 400 kA·m^{-1}, the domain deflection at grain boundary is basically completed, and the demagnetization curve is still full. With the increase in the reverse magnetic field up to $-$ 560 kA·m^{-1}, some coarser magnetic domains in regions with low Cu content begin to deflect. When the reverse magnetic field increases to $-$ 800 kA·m^{-1}, the cluster-like reverse domain begins to enlarge gradually, as shown in Fig. 4g. At the reverse magnetic field of $-$ 1120 kA·m^{-1}, the cluster-like reverse domain enlarges further and coarser domain regions almost

completely reverse. The inversion process of the magnetic domain is consistent with its corresponding demagnetization curve. For the 2:17-type SmCo magnets, the thinner the domain width is, the stronger the pinning force will be, as shown in Fig. 4b. Therefore, the high Cu content can enhance the ability of magnetic domains against the reversal magnetic field. As a result, increasing Fe content can lead to the inhomogeneous Cu distribution in the inner grain, which may be the main reason for the poor S_r of the M$_B$ magnet.

The samples with c-axis perpendicular to the surface were selected for TEM analysis, and the results are shown in Fig. 5. Figure 5a and b shows microscopic morphology of different regions in M$_A$ magnet, and Fig. 5c and d shows
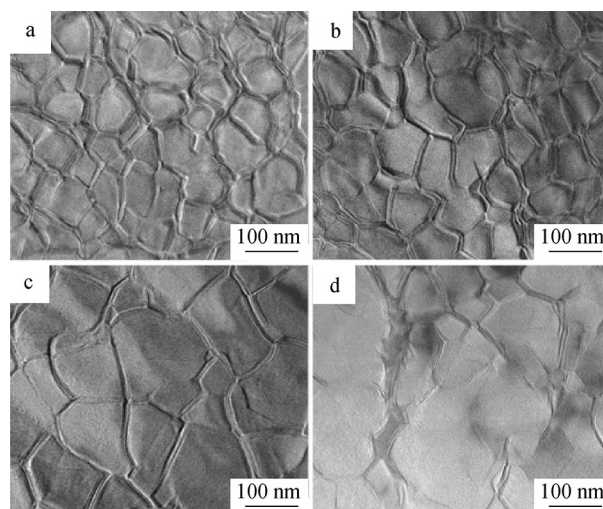

Fig. 5 TEM bright-field images of cellular structure along [0001]$_{2:17}$ zone axis in **a**, **b** M$_A$ magnet and **c**, **d** M$_B$ magnet

that in M_B magnet. It is established that the size of cell structures in M_A magnet is about 70 nm, which agrees with the results observed by EPMA and MOKE. However, the microstructures of different regions in M_B magnet are quite different. Complete cellular and cell boundary phase with an average size of 120 nm are observed in Fig. 5c, and incomplete cellular phases with an average size of 140 nm are obtained in Fig. 5d. The average size of the cellular phase in M_B magnet is much larger than that in M_A magnet, which can be attributed to their different Fe contents. It is noticed that the smaller average cell size in M_A magnet is one of the reasons for the higher H_{cj}. Furthermore, the corresponding observations of EPMA and TEM indicate that the higher Sm and Cu contents can also prove the formation of more cell boundary phase, leading to the complete cellular phase as well as narrower magnetic domain, as shown in Figs. 4b and 5c. The effect of increasing Fe content is proved to be twofold by our further investigations. On the one hand, the increase in Fe content can promote the growth of the cellular phase. And on the other hand, it can cause the inhomogeneous elemental distribution in the inner grains, leading to the incomplete cell boundary phase and coarser magnetic domain in some regions with lower Cu content.

4 Conclusion

The effect of elemental distribution on microstructure of $Sm(Co_{bal}Fe_{0.15}Cu_{0.07}Zr_{0.03})_{7.8}$ and $Sm(Co_{bal}Fe_{0.28}Cu_{0.07}Zr_{0.03})_{6.6}$ magnets was investigated. Experimental results show that magnets with higher Fe content are more sensitive to the change in solid solution temperature. The completeness of cell boundary phase and corresponding magnetic domain width are determined by the local Cu content. The EPMA and MOKE results indicate that the regions with higher Cu content have narrower magnetic domains, leading to the stronger resistance during demagnetization stage. Furthermore, the in-situ observation of EPMA and MOKE provides an effective way to discuss the relationship between microstructure and magnetic properties.

References

[1] Liu JF, Chui T, Dimitrov D, Hadjipanayis GC. First-principle studies of Sm–Co hard magnets. Appl Phys Lett. 1998;73(20):3007.

[2] Liu S, Yang J, Doly G, Euhl GE, Chen C, Walmer M, Simon G. New sintered high temperature Sm–Co based permanent magnet materials. IEEE Trans Magn. 1999;35(5):3325.

[3] Liu S, Potts G, Doyle G, Yang J, Euhl GE, Chen C, Walmer MS, Walmer MH. Effect of z value on high temperature performance of Sm(Co, Fe, Cu, Zr)$_z$ with z = 7.14–8.10. IEEE Trans Magn. 2000;36(5):3297.

[4] Chen CH, Gong W, Walmer MH, Liu S, Kuhl GE. Behavior of some heavy and light rare earth-cobalt magnets at high temperature. J Appl Phys. 2002;91(10):8483.

[5] Pragnell WM, Evans HE, Williams AJ. Oxidation protection of Sm$_2$Co$_{17}$-based alloys. J Alloy Compd. 2012;517:92.

[6] Xu C, Wang H, Zhang TL, Popov A, Gopalan R, Jiang CB. Correlation of microstructure and magnetic properties in Sm(Co$_{bal}$Fe$_{0.1}$Cu$_{0.1}$Zr$_{0.033}$)$_{6.93}$ magnets solution-treated at different temperatures. Rare Met. 2019;38(1):20.

[7] Bibi S, Wang JM, Rathore MF, Jiang CB. Temperature stability of SmCo (2:17) magnets modified by Ni–Cr two-layer coating. Rare Met. 2019;39(3):238.

[8] Liu JF, Hadjipanayis GC. Demagnetization curves and coercivity mechanism in Sm(CoFeCuZr)$_z$ magnets. J Magn Magn Mater. 1999;195(3):620.

[9] Yan A, Gutfleisch O, Handstein A, Gemming T, Müller KH. Microstructure, microchemistry, and magnetic properties of melt-spun Sm(Co, Fe, Cu, Zr)$_z$ magnets. J Appl Phys. 2003;93(10):7975.

[10] Xiong XY, Ohkubo T, Koyama T, Ohashi K, Tawara Y, Hono K. The microstructure of sintered Sm(Co$_{0.72}$Fe$_{0.20}$Cu$_{0.055}$Zr$_{0.025}$)$_{7.5}$ permanent magnet studied by atom probe. Acta Mater. 2004;52(3):737.

[11] Feng HB, Chen HS, Guo ZH, Yu RH, Li W. Twinning structure in Sm(Co, Fe, Cu, Zr)$_z$ permanent magnet. Intermetallics. 2010;18(5):1067.

[12] Ojima T, Tomizawa S, Yoneyama T, Hori T. New type rare earth cobalt magnets with an energy product of 30 MGOe. Jpn J Appl Phys. 1977;16(4):671.

[13] Ojima T, Tomizawa S, Yoneyam T, Hori T. Magnetic properties of a new type of rare-earth cobalt magnets Sm$_2$(Co, Cu, Fe, M)$_{17}$. IEEE Trans Magn. 1977;13(5):1317.

[14] Liu S, Ray AE. Sm$_2$(Co, Fe, Cu, Zr)$_{17}$ magnets with higher Fe content. IEEE Trans Magn. 1989;25(5):3785.

[15] Ma BM, Liang YL, Patel J, Scott D, Bounds CO. The effect of Fe content on the temperature dependent magnetic properties of Sm(Co, Fe, Cu, Zr)$_z$ and SmCo$_5$ sintered magnets at 450°C. IEEE Trans Magn. 1996;32(5):4377.

[16] Horiuchi Y, Masaya ME, Naoyuki S, Shinya S. Influence of intermediate-heat treatment on the structure and magnetic properties of iron-rich Sm(CoFeCuZr)$_z$ sintered magnets. J Appl Phys. 2015;117(17):17C704.

[17] Song KK, Fang YK, Sun W, Chen HS, Yu NJ, Zhu MG, Li W. Microstructural analysis during the step-cooling annealing of iron-rich Sm(Co$_{0.65}$Fe$_{0.26}$Cu$_{0.07}$Zr$_{0.02}$)$_{7.8}$ anisotropic sintered magnets. IEEE Trans Magn. 2017;53(11):2100804.

[18] Song KK, Sun W, Chen HS, Yu NJ, Fang YK, Zhu MG, Li W. Revealing on metallurgical behavior of iron-rich Sm(Co$_{0.65}$Fe$_{0.26}$Cu$_{0.07}$Zr$_{0.02}$)$_{7.8}$ sintered magnets. AIP Adv. 2017;7(5):056238.

[19] Kronmüller H, Goll D. Micromagnetic analysis of pinning-hardened nanostructured, nanocrystalline Sm$_2$Co$_{17}$ based alloys. Scripta Mater. 2002;47(8):545.

[20] Zhang Y, Tang W, Hadjipanayis GC, Chen C, Nelson C, Krishnan K. Evolution of microstructure, microchemistry and coercivity in 2–17 type Sm–Co magnets with heat treatment. IEEE Trans Magn. 2001;37(4):2525.

[21] Xiong XY, Ohkubo T, Koyama T, Ohashi K, Tawara Y, Hono K. The micro-structure of sintered Sm(Co$_{0.72}$Fe$_{0.20}$C$_{u0.055}$Zr$_{0.}$

$_{025})_{7.5}$ permanent magnet studied by atom probe. Acta Mater. 2004;52(3):737.

[22] Tian Y, Liu ZH, Xu H, Du J, Zhang J, Xia WX, Che RC, Yan AR, Liu JP. In situ observation of domain wall pinning in Sm(Co, Fe, Cu, Zr)$_z$ magnet by Lorentz microscopy. IEEE Trans Magn. 2015;51(11):2102404.

[23] Wang YQ, Shang ZF, Yue M, Wu D, Zhang DT, Zhang HG, Liu WQ. Correlation between Fe content and z value in Sm(Co$_{bal}$Fe$_x$Cu$_{0.06}$Zr$_{0.025}$)$_z$ permanent magnets. J Magn Magn Magn. 2019;474:417.

[24] Guo ZH, Pan W, Li W. Sm(Co, Fe, Cu, Zr)$_z$ sintered magnets with a maximum operating temperature of 500 °C. J Magn Magn Mater. 2006;303(2):396.

[25] Tang W, Zhang Y, Hadjipanayis GC. High-temperature magnetic properties of Sm(Co$_{bal}$Fe$_{0.1}$Cu$_{0.088}$Zr$_x$)$_{8.5}$ magnets. J Magn Magn Mater. 2000;221(3):268.

[26] Huang MQ, Zheng Y, Wallace WE. SmCo(2:17-type) magnets with high contents of Fe and light rare earths. J Appl Phys. 1994; 75(10):6280.

[27] Zhang Y, Corte-Real M, Hadjipanayis GC. Magnetic hardening studies in sintered Sm(Co, Cu$_x$, Fe, Zr)$_z$ 2:17 high temperature magnets. J Appl Phys. 2000;87(9):6722.

[28] Zhang TL, Song Q, Wang H, Wang JM, Liu JH, Jiang CB. Effects of solution temperature and Cu content on the properties and microstructure of 2-17 type SmCo magnets. J Alloys Compd. 2018;735:1971.

[29] Wang YQ, Yue M, Wu D, Zhang DT, Liu WQ, Zhang HG. Microstructure modification induced giant coercivity enhancement in Sm(CoFeCuZe)$_z$ permanent magnets. Scripta Meter. 2018;146:231.

[30] Wang GJ, Jiang CB. The coercivity and domain structure of Sm(Co$_{bal}$Fe$_{0.1}$Cu$_x$Zr$_{0.033}$)$_{6.9}$ ($x = 0.07, 0.10, 0.13$) high temperature permanent magnets. J Appl Phys. 2012;112(3):033909.

[31] Yan A, Gutfleisch O, Gemming T, Müller KH. Microchemistry and magnetization reversal mechanism in melt-spun 2:17-type Sm–Co magnets. Appl Phys Lett. 2003;83(11):2208.